Dopamine Adsorption on Rutile TiO_2(110): Geometry, Thermodynamics, and Core-Level Shifts from First Principles

Noemi Cadmen, Joana Bustamante, Richard Rivera, F. Javier Torres*, and Jorge Ontaneda*

Cite this: *ACS Omega* 2022, 7, 5, 4185–4193
Publication Date: January 28, 2022
https://doi.org/10.1021/acsomega.1c05784

Abstract

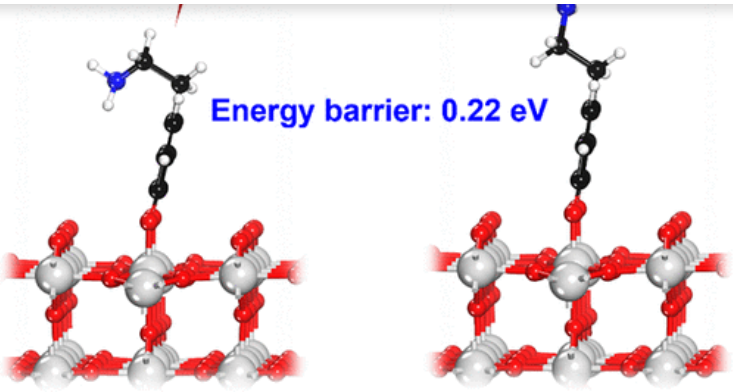

The modification of the rutile TiO_2(110) surface with dopamine represents the best example of the functionalization of TiO_2-based nanoparticles with catecholamines, which is of great interest for sunlight harvesting and drug delivery. However, there is little information on the dopamine–TiO_2(110) adsorption complex in terms of thermodynamic properties and structural parameters such as bond coordination and orientation of the terminal ethyl–amino group. Here, we report a density functional theory (DFT) investigation of dopamine adsorption on the TiO_2(110) surface using the optB86b-vdW functional with a Hubbard-type correction to the Ti 3d orbitals, where U_{eff} = 3 eV. Guided by available X-ray photoelectron spectroscopy (XPS) and near-edge X-ray absorption fine structure (NEXAFS) data, our simulations identify enolate species with bidentate coordination at a submonolayer coverage, which are bonded to two neighboring 5-fold-coordinated Ti atoms at the TiO_2(110) surface through both deprotonated oxygen atoms of the dopamine, i.e., in a bridging fashion. The process is highly exothermic, involving an adsorption energy of −2.90 eV. Calculated structural parameters suggest that the molecule sits approximately upright on the surface with the amino group interacting with the π-like orbitals of the aromatic ring, leading to a gauche-like configuration. The resulting NH···π hydrogen bond in this configuration can be broken by overcoming an energy barrier of 0.22 eV; in this way, the amino group rotation leads to an anti-like conformation, making this terminal group able to bind to other biomolecules. This mechanism is endothermic by 0.07 eV. Comparison of existing spectroscopic data with DFT modeling shows that our computational setup can reproduce most experimentally determined parameters such as tilt angles from NEXAFS and chemical shifts in XPS, which allows us to identify the preferred mode of adsorption of dopamine on the TiO_2(110) surface.

1. Introduction

Jump To

The functionalization of TiO_2 nanomaterials is of significant interest to many applications, including photovoltaics, (1) photocatalysis, (2) and nanomedicine. (3) Organic molecules are commonly used to modify the surfaces of TiO_2 nanostructures to allow tuning of the band

organic molecules, including polymers, proteins, and DNA fragments. Such a functionalization leads to the development of novel bioinorganic hybrid nanoconjugates, (3,5) which can be used in biomedical applications such as the targeting of specific cells and multimodal imaging. (6−9)

Catecholamines, a family of organic compounds that have a catechol and a side-chain amine, are surface modifiers for TiO_2 that provide specific binding sites for biomolecules. (10−12) These compounds act as a linker with one of the functionals anchoring the surface of the metal oxide and the other binding the bioactive molecule. Dopamine, for example, contains a vicinal diol in the catechol-like portion for surface anchoring and one ethyl−amino group for bioactive molecule binding. In fact, both functional groups facilitate the charge transfer between the TiO_2 nanomaterial and the biological component, as evidenced in the work of Liu et al., (10) where a method to control charge transfer from DNA to TiO_2/dopamine is proposed. This type of nanoconjugate has been considered in gene knockout devices and tumor imaging agents. (13)

In order to optimize the syntheses and applications of dopamine-functionalized TiO_2 nanohybrids, it is desirable to gain a complete atomistic understanding of the bonding environment of the dopamine adsorbed on TiO_2 surfaces. Most of this knowledge comes from experimental (14) and theoretical (15,16) studies of the anatase TiO_2(101)−dopamine interfaces. The experimental work of Syres et al. (14) devoted to this interface has been carried out via X-ray photoelectron spectroscopy (XPS), ultraviolet photoelectron spectroscopy (UPS), and near-edge X-ray absorption fine structure spectroscopy (NEXAFS). According to this work, dopamine bonds through the deprotonated oxygen atoms of vicinal diols to the five-coordinated titanium atoms at the anatase TiO_2(101) surface, with the plane of the ring at around 90° from the surface. However, the data cannot say whether dopamine bonds through both oxygens to two neighboring surface Ti atoms (bridging) or both oxygen atoms in dopamine bonds to a single surface Ti atom (chelating). Results coming from theoretical investigations, however, identified the bridging bidentate fashion as the preferred mode of adsorption for this system. (15,16) Also, thermodynamic and kinetic aspects, such as adsorption energies and growth conditions, are covered. (15)

Jackman et al., (17) on the other hand, studied the adsorption complex of rutile TiO_2(110) and dopamine using XPS and NEXAFS. It was determined that dopamine adsorbs dissociatively on the rutile TiO_2(110) surface following deprotonation of the alcohol groups in a similar fashion with the anatase TiO_2(101) surface. According to the NEXAFS data reported in that study, the ring plane of dopamine is tilted 78 ± 5° away from the surface and twisted roughly 11 ± 5° off the (001) direction. Similarly to the anatase case, the XPS measurements are not able to distinguish between bridging and chelating modes of adsorption. The early theoretical study of Castillo et al. (18) determined that dopamine sits approximately normal to the surface in agreement with ref (17). However, adsorption energies and the bonding

the advantages of exploiting a linker with double functional moieties. (6,10,12,13)

In this work, we employ density functional theory (DFT) modeling to gain further insights into the rutile TiO_2(110)–dopamine adsorption complex. Our calculations are based on the experimental output reported in ref (17), which allows us to make a direct comparison.

2. Results and Discussion

Jump To

2.1. Gas-Phase Dopamine

Dopamine belongs to the catecholamine family whose chemical formula is $C_6H_3(OH)_2$–$CH_2CH_2NH_2$. It consists of one amino group attached via an ethyl chain to a catechol structure—a benzene ring with two hydroxyl groups. Therefore, it is the simplest possible catecholamine. Dopamine exhibits high flexibility, which results in a significant number of conformations. Cabezas et al. (19) performed a detailed conformational search of dopamine in the gas phase (where it adopts a neutral form) employing laser-ablation molecular-beam Fourier transform microwave (LA-MB-FTMW) spectroscopy in combination with Møller–Plesset second-order perturbation method (MP2) simulations. A total of 18 candidates were proposed for the dopamine molecule, which are divided into two groups according to the orientation of the side-chain amine: gauche (G) and anti (A). Of these, seven conformers were observed in the gas phase by the spectroscopic technique, all of them corresponding to a gauche-type configuration.

We only considered the lowest-energy configuration of gas-phase dopamine from the above groups to be calculated with our computational setup. Figure 1 displays the spatial configuration of the two conformers after optimization. Dopamine in the gas phase is stabilized by a NH···π interaction between the amino group and the π-orbitals of the aromatic ring, which, judged by the N-O1 distance whose value is 6.354 Å, results in a folded structure (Conformer G). When dopamine is extended (Conformer A, N-O1 distance = 7.857 Å) such that this polar intramolecular interaction is not present anymore, the relative energy decreases by 0.07 eV. Our result compares very well with the relative energies at the MP2 level reported in ref (19), which was estimated as 0.07 eV (526 cm^{-1}). The PBE functional, on the other hand, predicts that Conformer A is more stable than Conformer G by 0.63 eV, which is expected since weak hydrogen bonding is not properly accounted within this approach.

Figure 1

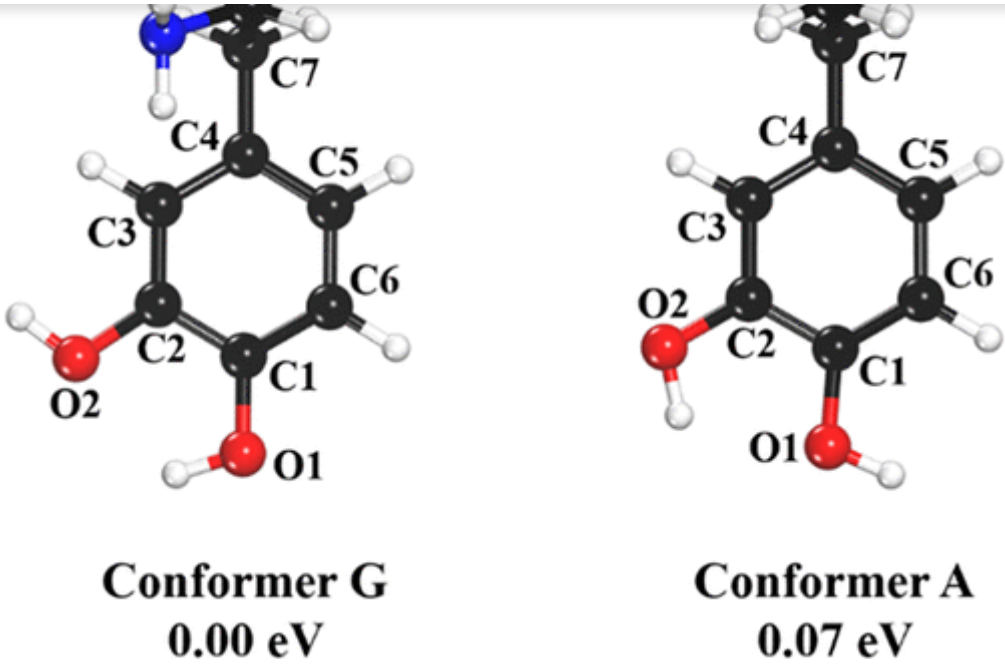

Figure 1. Molecular structure of the lowest-energy conformers of gaseous dopamine, according to the optB86b-vdW functional. Refer to Table S1 for numerical values of the bond lengths and angles. The white, black, blue, and red spheres denote the H, C, N, and O atoms, respectively.

The existence of stabilizing the NH···π hydrogen bond envisaged by the optB86b-vdW functional has been confirmed by LA-MB-FTMW via ^{14}N nuclear quadrupole coupling interactions. (19) This weakly polar intramolecular interaction is the force that drives the conformational preference not only in gas-phase dopamine but also in other neurotransmitters like 2-phenylethylamine (20) and serotonin. (21)

Since Conformer G is the most stable configuration, we use it in eq 1 as the reference for the calculation of adsorption energies. For the other two tested functionals, we selected the lowest-energy configuration of dopamine in each situation regardless of the order of stability. In any case, the selection of reference is largely arbitrary as our focus is the relative stability of the different adsorption configurations.

2.2. Relaxations in the Clean TiO_2(110) Surface

Rutile TiO_2(110) surface termination exhibits both titanium and oxygen species with two different types of coordination, as illustrated in Figure 2. Along the (001) direction, rows of 6-fold-coordinated Ti atoms (Ti_{6f}) alternate with 5-fold-coordinated Ti atoms (Ti_{5f}) separated by rows of O species, which are 3-fold coordinated as in the bulk and commonly referred as in-plane O atoms (O_{ip}). The former of the Ti atoms are covered by rows of two-fold-coordinated O species or bridging O atoms (O_{br}), whereas the latter are exposed to the surroundings. Upon relaxation, the two types of oxygen atoms and the Ti_{6f} species move

Figure 2

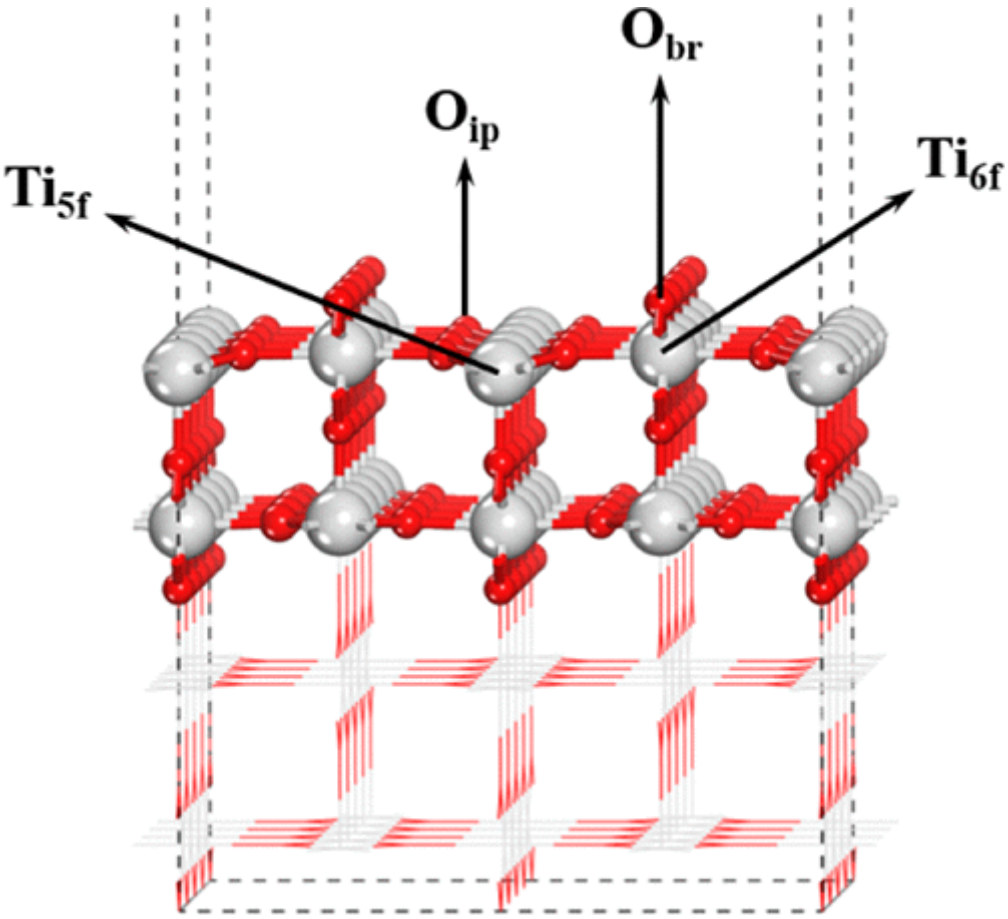

Figure 2. Schematic representation of the TiO_2(110) surface illustrating the 5- and 6-fold-coordinated Ti species together with the in-plane and bridging O atoms. Ball-and-stick (line) style depicts the relaxed (frozen) part of the asymmetric slab model used in this study. Red and gray colors correspond to O and Ti atoms, respectively.

In Table 1, we present the calculated displacements predicted by the optB86b-vdW functionals contrasted with available experimental data as reported by quantitative low energy electron diffraction (LEED-IV), (22) surface X-ray diffraction (SXRD), (23) and scanned-energy mode photoelectron diffraction (PhD). (24) In general, our calculations are qualitatively consistent with the three sets of experiments, even considering the significant error values estimated in the PhD study. In this context, comparison has been made around LEED-IV and SXRD. According to Table 1, the downward displacement of the Ti_{5f} layer and the upward relaxation of the O_{ip} species are in excellent agreement with both experimental studies, particularly with those determined by SXRD. The calculated values for the positive relaxations of both the Ti_{6f} and O_{br} atoms are a little shorter than those estimated by LEED-IV and SXRD measurements, where a good agreement is seen between the two sets of results. The only significant difference between our simulations and the experiment accounted by

from the optB88-vdW functional as reported by Tillotson et al., (25) where parameter U_{eff} = 3 eV was applied for the 3d states as well (see Table 1). We can see that although the performance of these two nonlocal functionals is similar (as their exchange parts are closely defined), the optB86b-vdW functional provides slightly better results at reproducing relaxations in the TiO_2(110) surface, especially when comparing with SXRD results. (23) This conclusion was also attained in ref (26) on studying atomic displacements in this surface with different nonlocal functionals but without including any Hubbard-type correction.

Table 1. Calculated Atomic Displacements (Å) along the (110) Direction in Comparison with Available Experimental Data[f]

	optB86b-vdW	optB88-vdW	LEED-IV[c]	SXRD[d]	PhD[e]
Ti_{6f}	0.19, 0.34[a]	0.40,[a] 0.17[b]	0.25 ± 0.03	0.25 ± 0.01	0.19 (−0.15
Ti_{5f}	−0.12, −0.18[a]	−0.15,[a] −0.15[b]	−0.19 ± 0.05	−0.11 ± 0.01	−0.26 ± 0.0
O_{ip}	0.17, 0.18[a]	0.22,[a] 0.14[b]	0.27 ± 0.08	0.17 ± 0.03	0.00 (−0.40
O_{br}	0.02, 0.15[a]	0.20,[a] 0.01[b]	0.10 ± 0.05	0.10 ± 0.04	0.17 ± 0.15

[a]Reference (26) (E_{cutoff} = 700 eV, without Hubbard correction).
[b]Reference (25) (E_{cutoff} = 400 eV, U_{eff} = 3 eV).
[c]Reference (22).
[d]Reference (23).
[e]Reference (24).
[f]Previous theoretical work on these parameters is also contrasted. Positive and negative value displacements indicate upward and downward relaxations, respectively. For atom illustrations, see Figure 2.

Since optB86b-vdW provides a robust description of both the adsorbate and the substrate, we used it here to study the dopamine-TiO_2(110) adsorption complex at an atomistic level.

2.3. Exploration of the Configurational Space for the Dopamine–TiO_2(110) Adsorption Complex

Similar to catechol, the hydroxyl groups in dopamine are susceptible to deprotonation, yielding dopamine enolates plus one or two protons. On the basis of the acid–base adsorption mechanism on metal oxides, (27) oxygen atoms of the adsorbate can form bonds with the acidic sites of the substrate (cations) while the protons of the molecule

the whole process can result into two dissociative adsorption modes: monodentate (only one oxygen binds to the surface) and bidentate (both oxygens form bonds with the substrate). As reported in ref (17), XPS measurements determined (i) the presence of deprotonated species only at a sub-monolayer regime and (ii) dopamine bonds in a bidentate fashion. Therefore, we only considered bidentate modes of adsorption, placing the two protons as far as possible from the adsorption sites (refer to Supporting Information for further analysis).

We did not consider configurations where dopamine bends toward the surface to allow interaction of the NH_2 group with the surface as reported in the recent theoretical investigation by Ronchi et al., (15) who studied dopamine adsorption on anatase TiO_2(101) surfaces at low coverages. In this system, the topology of the substrate facilitates this additional interaction between the terminal ethyl–amino group (via the N atom) and a Ti_{5f} species located at the underlying sawtooth-like structure. (28) This might not be the case for the rutile TiO_2(110) surface. Indeed, the available NEXAFS data at a sub-monolayer regime reported in ref (17) clearly indicates that the angle for the π* vector-like orbitals is almost parallel to the surface, which means that dopamine sits approximately normal to the surface. Thus, it is unlikely to see deprotonated dopamine motifs bending toward the rutile TiO_2(110) surface to promote such an interaction, at least not at the experimental conditions referenced in this study, which guided our investigation.

The configurational space of dissociative adsorption in a bidentate fashion comprises two modes: bridging (each oxygen in dopamine bonded to neighboring Ti_{5f} atoms) and chelating (both oxygen atoms bonding to a single Ti_{5f} atom). We also considered both conformers (gauche and anti) of dopamine in the gas phase. In total, four configurations were generated, which, after geometry optimization, are depicted in Figure 3. According to our simulations, the adsorption of dopamine on TiO_2(110) surfaces is highly exothermic for all four candidates, with adsorption energies ranging from −1.40 to −2.90 eV. In bridging and chelating fashions, gauche (G) and anti (A) configurations have similar adsorption energies which could mean that from a thermodynamical point of view, both structures are allowed to coexist/compete and that overall, bridging modes of adsorption are more favorable than those adopting a chelating configuration.

Figure 3

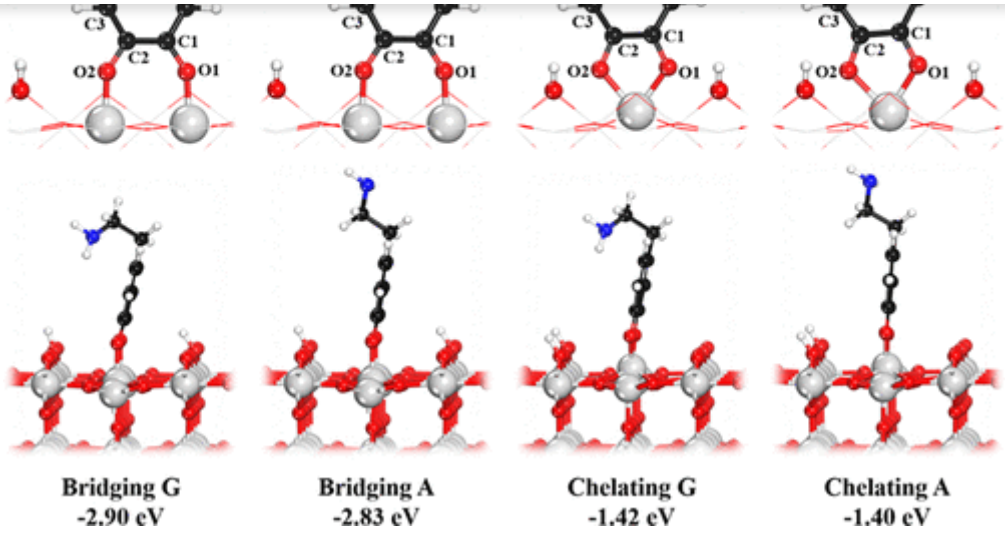

Figure 3. Adsorption configurations of dopamine over the TiO_2(110) surface considered in the present study. The candidates illustrated here were optimized within the optB86b-vdW approach. Final geometries via the optB88-vdW and PBE functionals were essentially the same. Refer to Table S2 in Supporting Information for the calculated values from the optB88-vdW and PBE simulations. Oxygen and carbon atoms are numbered in line with Figure 1 and with the results of core-level shift calculations listed in Table 3.

This general trend is also observed with the optB88-vdW and PBE functionals, as seen in Table S2 of the Supporting Information. The relative values within the optB88-vdW (optB86b-vdW) approach indicate that “Bridging G” is more stable than “Bridging A” by only 0.03 (0.07) eV, while “Chelating G” and “Chelating A” differ by 0.04 (0.02) eV in the same order of stability. Considering the lowest-energy configuration in each case, bridging is favored over chelating by 1.45 (1.48) eV. Similar relative values were obtained by the standard PBE functional: “Bridging G” > “Bridging A” by 0.03 eV, “Chelating G” > “Chelating A” by 0.01 eV, and bridging > chelating by 1.28 eV. Therefore, our results are largely consistent among the DFT functionals considered in the present study.

However, PBE calculates lower values for the adsorption energy of dopamine over the TiO_2(110) surface than both nonlocal functionals. According to Table S2, the adsorption energy of the most stable configuration computed by the PBE functional is −1.95 eV, which is significantly much lower than those from optB86b-vdW (−2.90 eV) and optB88-vdW (−2.83 eV) functionals. On average, the inclusion of dispersion in terms of nonlocal correlation increases the strength of dopamine adsorption onto the TiO_2(110) surface by ∼0.9 eV. A significant contribution of vdW interactions to the adsorption energy has been also observed for the dissociative adsorption of small organic molecules on this surface, like formic acid and glycine, with calculated values up to ∼0.6 eV. (25) However, these adsorption energies might be overestimated due to the significant differences between experiment and theory, as found in the case of methanol. (25,26) In any case, our results show that the order of stability

Overall, the most important result in this section is that, according to Figure 3, Bridging G is rendered as the most stable configuration among the four candidates. Owing to the number of contacts present, bridging bidentate configurations were a priori presumed to be the preferable mode of adsorption for dopamine over the rutile TiO_2(110) surface. Actually, such configurations have been determined for oxygen-legged compounds adsorbed on this TiO_2 surface, (28,29) including catechol (30,31) and benzoate. (32) Nevertheless, it is noteworthy to point out two facts. First, all candidates feature very negative adsorption energies and therefore could represent local minima in the potential energy landscape, and second, the tiny difference in energy between "Bridging G" and "Bridging A" configurations makes difficult the task of making an unambiguous discrimination based on adsorption energies alone; it is likely that both candidates coexist with a small transition barrier between them. Consequently, we need to refer to available experimental data in comparison with our DFT results in order to make a reliable determination of the adsorption complex.

2.4. Comparison of DFT Modeling with Available Experimental Data

As illustrated in Figure 4, we determined the tilt angles of the benzene ring with respect to the surface plane (α) and with respect to the row of bridging oxygen atoms along the (001) direction (β). In the experimental work by Jackman et al., (17) angle-resolved NEXAFS spectra determined both angles as α = 78° and β = 11° (with a margin of error of 5°), which indicate the dopamine sits almost upright on the surface and slightly twisted with respect to the (001) direction. According to our simulations as summarized in Table 2, the α value is best reproduced in the "Bridging G" configuration, where α is off by 1° with respect to the experiment. In relation to the β parameter, "Chelating G" exhibits the best degree of agreement; in this case, β is perfectly reproduced by our simulations. In any case, the α and β values for both bridging modes and the "Chelating G" configuration are within the confidence interval of the experimental measurements, which implies that these tree configurations cannot be ignored. However, this is not the case for the remaining candidate, "Chelating A," where it is possible to see that both structural parameters are not compatible with the NEXAFS data. Thus, on the grounds of molecular orientation, we can only exclude the "Chelating A" configuration with reasonable confidence.

Figure 4

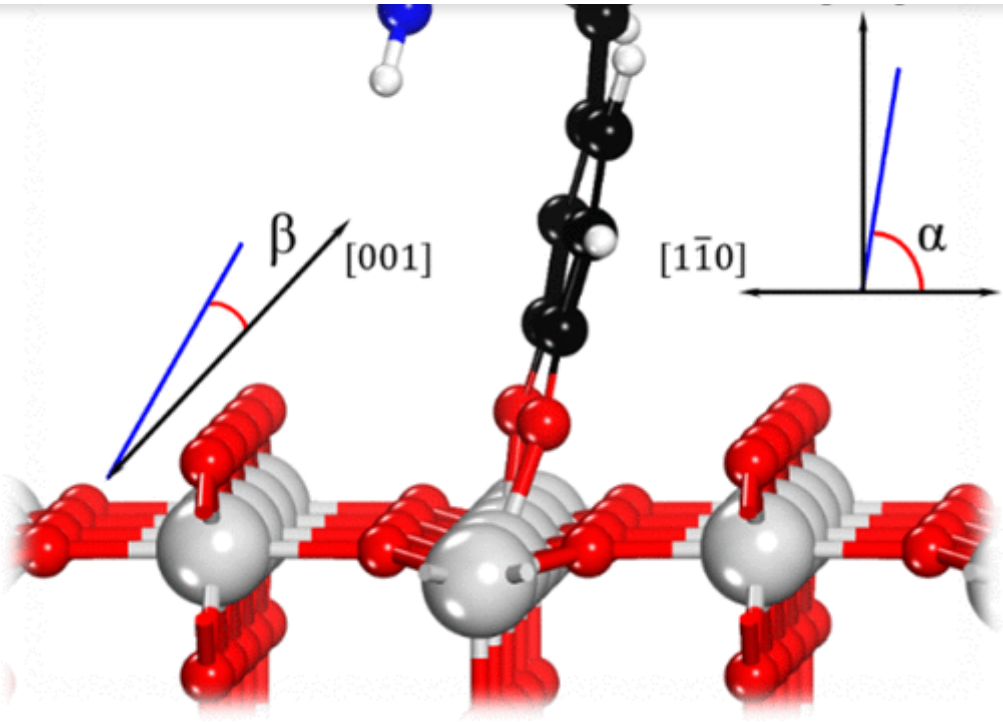

Figure 4. Schematic representation of adsorbed dopamine on the TiO_2(110) surface, defining the tilt angles α and β. Both are given with respect to the plane of the benzene ring.

Table 2. Key Structural Parameters of the Four Candidates as Determined by the optB86b-vdW Functional[b]

parameters	Bridging G	Bridging A	Chelating G	Chelating A	NEXAF
α	77°	81°	80°	86°	78 ± 5°
β	13°	9°	11°	5°	11 ± 5°
d(O1−Ti)	1.862 Å	1.859 Å	1.984 Å	1.959 Å	
d(O2−Ti)	1.868 Å	1.868 Å	2.014 Å	2.054 Å	
∠N−C8−C7−ring	63°	175°	63°	174°	

[a]Ref (17).
[b]For numbering, refer to Figure 3.

In addition to the tilt angles, we also computed the core-level shifts in the final state approximation, which can be contrasted against the binding energy (BE) shifts from the XPS data reported in ref (17). The recent work by Trinh et al. (33) demonstrated a synergistic

+ U approach is highly sensitive to the choice of the *U* parameter, which should be determined based on surface-dependent properties (like SXRD and XPS) rather than bulk properties. For the dopamine-TiO_2(110) system, U_{eff} = 3 eV seems to be a reasonable choice to capture most of the XPS features of the C 1s core levels, especially those arising from the benzene ring (C1–6), which were considered here to discriminate between bridging and chelating configurations as discussed further below.

Table 3 lists the calculated core-level shift values within the final state approximation for all candidates. The predicted relative shifts for the O 1s BEs are the same for all geometries, which is expected since the anchoring O atoms are in the same chemical environment, in turn making the task of discerning between bridging and chelating geometries difficult. On the other hand, C 1s BEs result in small shifts that allow us to make a reasonable discrimination. According to XPS data, (17) the C 1s photoemission peaks of C3, C5, and C6 indicate that they all have low BEs; so do the DFT values for all remaining candidates (even for "Chelating A," which was already discarded from the NEXAFS analysis). The C4 in all of them is shifted to a higher BE, which is also seen in the experimental data. The highest chemical shift in the C 1s BEs is experienced by C1 and C2 as reported by XPS. This shift is also seen in the tested geometries optimized with the optB86b-vdW functional, although its magnitude is off by ∼0.4 eV in the bridging fashion and ∼0.8 eV in the chelating fashion when comparing with XPS values. In relation to C7 and C8, they are also shifted to high BEs, but their sizes are not well reproduced by our simulations which, contrary to the experiment, are off by ∼1.3 and ∼1.4 eV, respectively.

Table 3. Relative Chemical Shifts in the O 1s and C 1s Binding Energies of Dopamine Adsorbed on the TiO_2(110) Surface[b]

	Bridging G	Bridging A	Chelating G	Chelating A	XPS[a]
ΔBE (O1)	0.0	0.0	0.0	0.0	0.0
ΔBE (O2)	0.0	0.0	0.0	0.0	0.0
ΔBE (C1)	1.5	1.4	1.2	1.1	1.9
ΔBE (C2)	1.5	1.5	1.2	1.2	1.9
ΔBE (C3)	0.0	0.0	0.0	0.0	0.0

ΔBE (C6)	0.0	0.0	0.1	0.0	0.0
ΔBE (C7)	1.9	1.9	1.9	1.9	0.6
ΔBE (C8)	3.0	3.0	3.2	3.1	1.6

[a]Ref (17).
[b]Values were obtained with the optB86b-vdW functional. See Figure 3 for atom numbering.

Note that none of the candidates is compatible with the available XPS data for the ethyl chain (C7 and C8). Considering the electronegativity of C, N, and O, C7 ($H_2C–CH_2NH_2$) should be shifted to a much lower C 1s BE, and C8 ($H_2C–NH_2$) should be shifted to a slightly lower C 1s BE compared to those of C1 and C2 (C–O). In fact, for the most stable configuration (Bridging G), this succession is roughly seen in the core-level shift calculations within the initial state approximation (Table S3), which only considers shifts arising from the change in the local environment of atoms. However, when core-hole screening contributions are incorporated as described in the final state calculations, both C7 and C8 are shifted to higher BEs compared to those of C1 and C2 (Table 3). It is clear that the energy relaxation due to the screening of the core hole left behind during the photoemission process dominates the chemical shifts in the ethyl chain (i.e., final state effects). We have checked that these chemical shifts are not associated to electron density redistribution upon adsorption: our Bader analysis for “Bridging G” shows that the net atomic charge for C7 and C8 in adsorbed dopamine remains the same despite the charge transfer occurring from adsorbate to substrate, which is calculated as 0.45 *e* (Table S4). It is likely that the assignment of the fitted peaks to the ethyl chain in the XPS spectrum of C 1s for dopamine adsorbed on the rutile TiO_2(110) surface was based on a negligible contribution from the final state effects, which might explain the discrepancy between experiment and theory regarding the relative chemical shifts in the C 1s BEs for C7 and C8. Moreover, such a spectrum displays a broad and complex line shape that does not allow a straightforward assignment and presumably a unique multiple-peak fitting (see Figure 2 in ref (17)). C1 1s spectra recorded for the adsorption of biomolecules over transition metals also exhibit a high degree of complexity, with multiple features coming from dissociation products formed upon adsorption, and are therefore difficult to resolve. (34−36)

Regarding the benzene ring (C1−6), Table S3 shows that the core-level shift values obtained with the initial and final state approaches are similar. The similarity between the two results implies that the character of the valence electron charge distribution (i.e., initial state effects) dominates the relative chemical shifts in the C 1s BEs. This correlation is important for the discrimination between bridging and chelating configurations because final state calculations can be directly compared with XPS measurements. Consequently, we focus our

configurations are in much better agreement with the experiment than their chelating counterparts regarding C1 and C2 (C–O). In other words, the comparison of experimental chemical shifts in the C 1s BEs with the theoretical values of our simulations suggests that the relative chemical shifts of the benzene ring (C1–6) are best reproduced in both bridging modes. Better yet, these configurations are also compatible with NEXAFS measurements as discussed above. Therefore, from this combined analysis, both chelating modes can be safely ignored as candidates.

2.5. Analysis of the Bonding Mode of the Dopamine Adsorbed on the TiO_2(110) Surface

At this point, it is still difficult to distinguish between “Bridging G” and “Bridging A” candidates with rational certainty since they both (i) are essentially isoenergetic and (ii) agree with available spectroscopic data. In order to understand the relationship between both bridging configurations, we investigated the transition from one to the other by means of the nudged band elastic (NEB) method (see Figure 5). The energy difference between “Bridging G” and “Bridging A” is 0.07 eV and can be associated with the strain energy of the “Bridging A” configuration. The two local minima are separated by an energy barrier of 0.22 eV, which means that the “Bridging G” configuration is the global minimum in the potential energy surface. The dihedral angle that determines the conformation of the side chain (∠N–C8–C7–ring) for the predicted transition state is 123°, which is roughly the average of the calculated values for “Bridging G” and “Bridging A” (see Table 2). From a kinetic point of view, it is possible to convert “Bridging G” (nonactivated structure) into “Bridging A” (activated structure) by overcoming this energetic barrier, which could be achieved under different experimental conditions and even at room temperature. (31) In this way, the NH···π hydrogen bond can be broken and dopamine might adopt an extended configuration, allowing the amino group to be ready to form hydrogen bonds with another system. After all, dopamine can be seen as a linker with double functional moieties: one anchoring the TiO_2(110) surface and the other binding a bioactive molecule. (3)

Figure 5

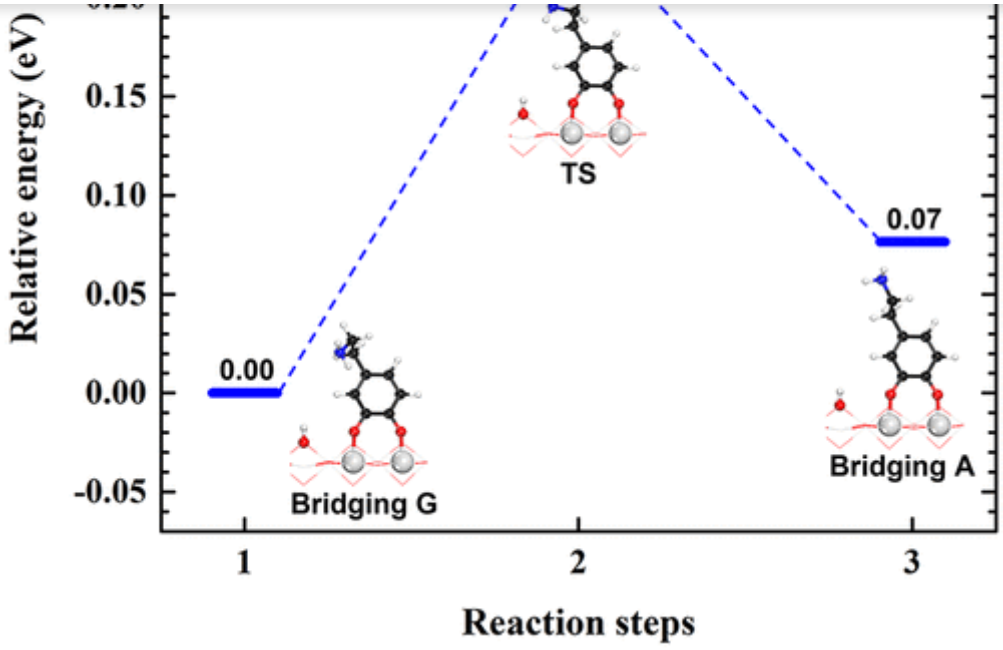

Figure 5. Nudged elastic band energy profile for converting Bridging G into Bridging A, as calculated with the optB86b-vdW functional.

As a final remark, the adsorption of dopamine over the rutile TiO_2(110) surface seems to be stronger than the case of catechol, the archetype of 1,2-dihydroxybenzene ligands. Within the PBE approximation, Li et al. (30) estimated the adsorption energy for low coverages (0.25 ML) of catechol adsorbed over the TiO_2(110) surface as −1.05 eV. For the dopamine–TiO_2(110) system in its most stable configuration, "Bridging G," our calculated PBE value (at a coverage of 0.125 ML) is −1.95 eV (see Table S2). This observation is also seen in the case of the anatase TiO_2(101) surface. (15) It is likely that this difference in adsorption energies arises from the presence of the amine side chain in the dopamine molecule, which also causes the dopamine to tilt away from the surface plane almost in an upright geometry. (14,17) Future research is in sight to evaluate the effect of other side-chain amines on the adsorption of catecholamines onto these surfaces.

3. Conclusions

Jump To

In summary, we performed DFT + U simulations to gain insights into the adsorption of dopamine on the rutile TiO_2(110) surface. To this purpose, we used the optB86b-vdW functional with the U_{eff} parameter set to 3 eV for the Ti 3d states. Our simulations indicate that dopamine is adsorbed dissociatively on the TiO_2(110) surface, following an acid–base adsorption mechanism: (27) deprotonated oxygens in the adsorbate bind to unsaturated Ti atoms, whereas protons move to the low-coordinated oxygens of the substrate. The adsorption process is highly exothermic by as much as −2.90 eV, and results in the formation of dopamine enolate species with bidentate coordination at the TiO_2(110) surface. According

for this system, bridging bidentate, suggested by the optB86b-vdW functional is also predicted by optB88-vdW and PBE, which demonstrates that our results are robust with respect to the choice of functional.

"Bridging G" is the lowest-energy configuration found in this theoretical work. In this geometry, the amino group interacts with the π-like orbitals of the benzene ring of the catechol-like part of dopamine, leading to a gauche-like configuration. An energy barrier of 0.22 eV is required to convert "Bridging G" into "Bridging A," in which the amino group is aligned with the ethyl chain axis leading to an anti-like conformation. This mechanism is endothermic by 0.07 eV and might allow the dopamine-functionalized TiO_2 nanomaterial to form hydrogen bonds with bioactive molecules via the terminal ethyl–amino group.

The calculated tilt angles for the "Bridging G" configuration are α = 77° and β = 13°, which are in excellent agreement with the NEXAFS analysis reported in ref (17) (78 ± 5° and 11 ± 5°, respectively). Additionally, the computed chemical shifts in the C 1s levels of the aromatic ring are in line with the XPS data reported in the same study, which can be seen in detail in Table 3. According to our core-level shift analysis based on initial and final state approximations, such chemical shifts are determined by initial state effects. Our DFT calculations also indicate that final state effects dominate the chemical shifts in the C 1s BEs in the ethyl chain.

Our results demonstrates that the optB86b-vdW functional, with a proper Hubbard-*U* term, is also able to reproduce most of the experimental features of the clean TiO_2(110) surface accounted by LEED-IV (22) and SXRD (23) and those of the dopamine-TiO_2(110) adsorption complex obtained via XPS and NEXAFS, (17) as evidenced in the present investigation.

4. Computational Methods

Jump To

We performed periodic DFT calculations using the plane-wave code VASP. (37,38) The interaction between the valence electrons and the core was treated within the projected augmented wave (PAW) method, (39,40) keeping the core electrons (1s in C, N, and O and up to 3p in Ti) frozen in the atomic reference configurations. The plane-wave basis in the simulations was truncated at a kinetic energy cutoff of 400 eV, which is the recommended value for the employed PAW potentials. To sample the Brillouin zone, we employed Monkhorst–Pack grids (41) with a maximum separation of 0.25 $Å^{-1}$ between k-points throughout the simulations. This grid density, which was found enough for convergence of the bulk rutile total energy, corresponds to 6 × 6 × 9 for the reciprocal space of the bulk.

The rutile TiO_2(110) surface was represented by a periodic slab of four O–Ti–O trilayers, which has been widely used in previous theoretical work of molecular adsorption on this

bottom ones were fixed in their optimized bulk positions; this procedure accelerates the convergence of calculated surface properties with respect to the thickness of the simulation slab. (25,44) The threshold for forces acting on ions during geometry optimizations was set to 0.01 eV $Å^{-1}$. Since we employed the asymmetric slab model, all simulations included a dipole correction as implemented in VASP based on a method proposed by Makov and Payne. (45) In our simulations, a vacuum gap of 20 Å separates each slab from its periodic images. Laterally, the supercell consisted of (4 × 2) surface unit cells; therefore, the adsorption of one dopamine molecule for every supercell corresponds to a surface coverage of 0.125 ML. This low coverage allows us to focus on the direct adsorbate–surface interactions rather than lateral interactions. Moreover, spectroscopic output reported in ref (17) was obtained at a sub-monolayer regime, which allows us also to make a much more reliable comparison with the experiment. For the simulation of the gas-phase dopamine, we used a large periodic cage, ensuring that each molecule is separated from its replicas by at least 12 Å.

We obtained geometries and total energies using the optB86b-vdW functional, where the dispersion is treated with explicit nonlocal correlation (46) as developed and implemented in VASP by Klimeš et al. (47) Output with both the generalized gradient approximation (GGA) in the form of the Perdew–Burke–Ernzerhof (PBE) exchange-correlation functional (48) and with the optB88-vdW functional (46) leads to essentially the same results in terms of relative adsorption energies for different configurations as discussed further below. For partly counteracting the artificial delocalization that results from the spurious electron self-interaction in DFT, (49) we applied a Hubbard-type correction (50) to the Ti 3d orbitals where parameter U_{eff} = 3 eV in both the nonlocal and semilocal functionals. This value has been commonly used in some previous theoretical studies of rutile (51,52) and anatase, (53,54) and as discussed below, it allows a rational description of most of the structural properties of the clean substrate as well as the O 1s and C 1s core levels of the adsorption complex.

For each adsorption configuration considered in the present investigation, we calculated the adsorption energy E_{ads}^{DFT} of dopamine on the TiO_2(110) surface as follows:

$$E_{ads}^{DFT} = E_{slab+molecule} - (E_{slab} + E_{molecule}) \quad (1)$$

where $E_{slab + molecule}$ is the energy of the optimized substrate–adsorbate system, E_{slab} denotes the energy of the relaxed clean TiO_2(110) surface, and $E_{molecule}$ corresponds to the energy of the gas-phase (intact) dopamine molecule at the lowest-energy configuration.

Finally, our core-level shift calculations were performed within the so-called final state approximation. (55) The core-level shifts obtained with this approach are estimated as total energy differences between two separate calculations as reported in ref (56). This procedure

considered instead. Such shifts are defined as the difference in binding energy of specific core-electrons BE_{CL} between an atom A and a reference atom A_{ref}:

$$\Delta BE_{CL}(A) = BE_{CL}(A) - BE_{CL}(A_{ref}) \quad (2)$$

We focused our discussion on the relative shifts of the C 1s levels of the carbon atoms of the adsorbed dopamine molecule, although O 1s level are also reported. In our investigation, we selected as reference atom the one yielding the lowest core-level binding energy in each case.

Supporting Information

Jump To

The Supporting Information is available free of charge at https://pubs.acs.org/doi/10.1021/acsomega.1c05784.

- Additional data from DFT calculations: geometrical properties of gas-phase dopamine, adsorption energies of all tested configurations within PBE and optB88-vdW functionals, analysis of the presence of co-adsorbed hydrogen on the surface, core-level shift calculations within the initial state approximation for the most stable configuration, and Bader charge analysis for the “Bridging G” configuration (PDF)

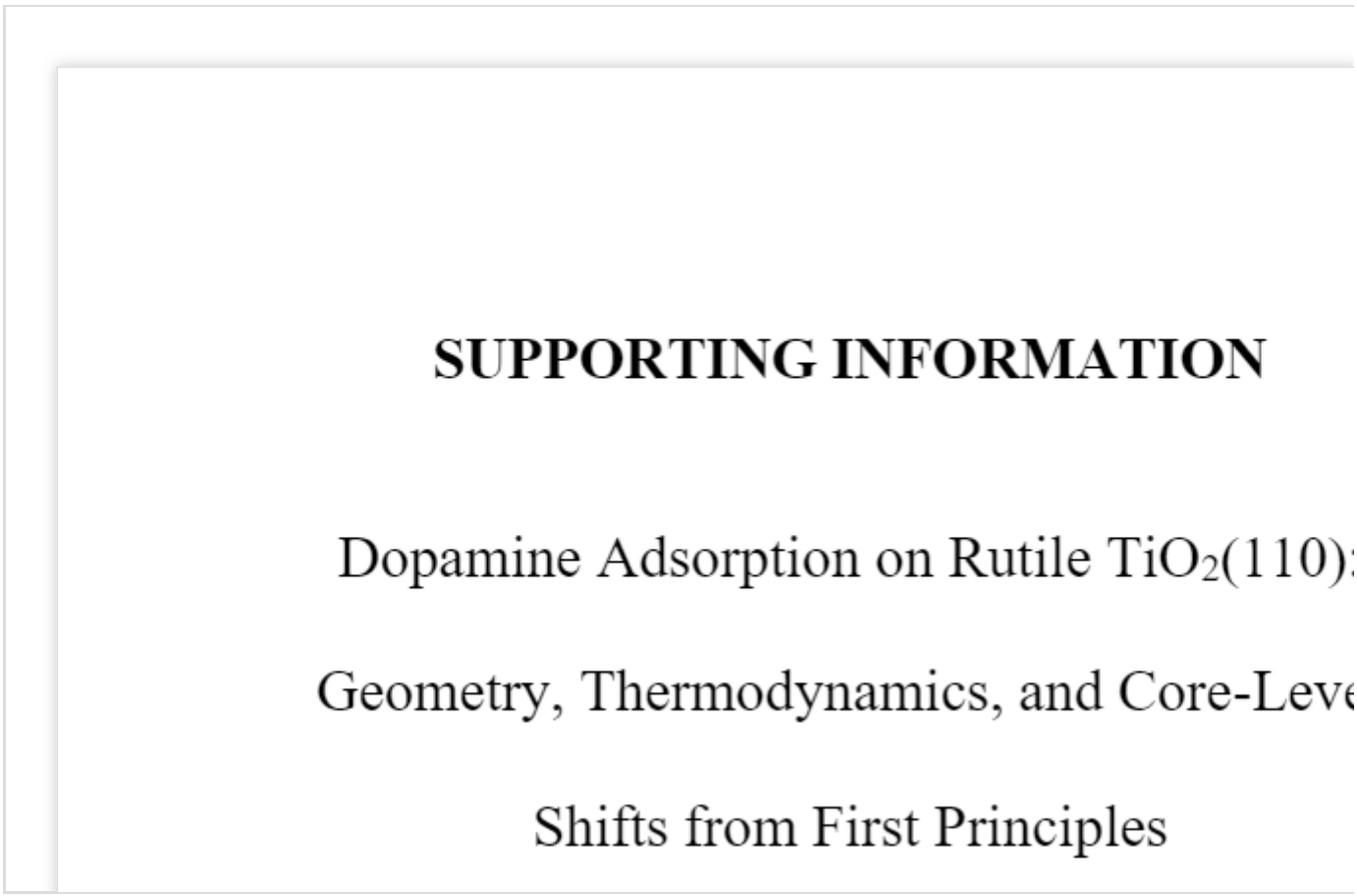

Terms & Conditions

Author Information

Jump To

Corresponding Authors

F. Javier Torres - *Grupo de Química Computacional y Teórica (QCT-UR), Facultad de Ciencias Naturales, Universidad del Rosario, Bogotá 111221, Colombia*; *Grupo de Química Computacional y Teórica (QCT-USFQ), Departamento de Ingeniería Química,*

San Cayetano Alto, Loja 1101608, Ecuador, Present Address: School of Engineering and Materials Science and Materials Research Institute, Queen Mary University of London, Mile End Road, London E1 4NS, United Kingdom;
https://orcid.org/0000-0003-1538-365X; Email: jeontaneda@utpl.edu.ec

Authors

Noemi Cadmen - *Departamento de Química, Universidad Técnica Particular de Loja, San Cayetano Alto, Loja 1101608, Ecuador*, https://orcid.org/0000-0002-2520-9527

Joana Bustamante - *Departamento de Química, Universidad Técnica Particular de Loja, San Cayetano Alto, Loja 1101608, Ecuador*, https://orcid.org/0000-0002-5469-3813

Richard Rivera - *Departamento de Química, Universidad Técnica Particular de Loja, San Cayetano Alto, Loja 1101608, Ecuador*, https://orcid.org/0000-0002-2285-1514

Notes

The authors declare no competing financial interest.

Acknowledgments

Jump To

This work has been performed by employing the resources of the high-performance computing systems of UTPL, USFQ, and UR. F.J.T. thanks the Alianza EFI-Colombia Científica grant with code 60185 and FP44842-220-2018.

References

Jump To

This article references 56 other publications.

1. Grätzel, M. Dye-Sensitized Solar Cells. *J. Photochem. Photobiol., C* **2003**, *4*, 145– 153, DOI: 10.1016/S1389-5567(03)00026-1 [Crossref], [CAS], [Google Scholar]

2. Henderson, M. A. A Surface Science Perspective on TiO_2 Photocatalysis. *Surf. Sci. Rep.* **2011**, *66*, 185– 297, DOI: 10.1016/j.surfrep.2011.01.001 [Crossref], [CAS], [Google Scholar]

3. Rajh, T.; Dimitrijevic, N. M.; Bissonnette, M.; Koritarov, T.; Konda, V. Titanium Dioxide in the Service of the Biomedical Revolution. *Chem. Rev.* **2014**, *114*, 10177– 10216, DOI: 10.1021/cr500029g [ACS Full Text], [CAS], [Google Scholar]

5. Wu, S.; Weng, Z.; Liu, X.; Yeung, K. W. K.; Chu, P. K. Functionalized TiO_2 Based Nanomaterials for Biomedical Applications. *Adv. Funct. Mater.* **2014**, *24*, 5464– 5481, DOI: 10.1002/adfm.201400706 [Crossref], [CAS], [Google Scholar]

6. Rajh, T.; Saponjic, Z.; Liu, J.; Dimitrijevic, N. M.; Scherer, N. F.; Vega-Arroyo, M.; Zapol, P.; Curtiss, L. A.; Thurnauer, M. C. Charge Transfer across the Nanocrystalline-DNA Interface: Probing DNA Recognition. *Nano Lett.* **2004**, *4*, 1017– 1023, DOI: 10.1021/nl049684p [ACS Full Text], [CAS], [Google Scholar]

7. Lopez, T.; Ortiz, E.; Alvarez, M.; Navarrete, J.; Odriozola, J. A.; Martinez-Ortega, F.; Páez-Mozo, E. A.; Escobar, P.; Espinoza, K. A.; Rivero, I. A. Study of the Stabilization of Zinc Phthalocyanine in Sol-Gel TiO_2 for Photodynamic Therapy Applications. *Nanomedicine* **2010**, *6*, 777– 785, DOI: 10.1016/j.nano.2010.04.007 [Crossref], [PubMed], [CAS], [Google Scholar]

8. Mano, S. S.; Kanehira, K.; Sonezaki, S.; Taniguchi, A. Effect of Polyethylene Glycol Modification of TiO_2 Nanoparticles on Cytotoxicity and Gene Expressions in Human Cell Lines. *Int. J. Mol. Sci.* **2012**, *13*, 3703– 3717, DOI: 10.3390/ijms13033703 [Crossref], [PubMed], [CAS], [Google Scholar]

9. Paunesku, T.; Rajh, T.; Wiederrecht, G.; Maser, J.; Vogt, S.; Stojićević, N.; Protić, M.; Lai, B.; Oryhon, J.; Thurnauer, M.; Woloschak, G. Biology of TiO_2-Oligonucleotide Nanocomposites. *Nat. Mater.* **2003**, *2*, 343– 346, DOI: 10.1038/nmat875 [Crossref], [PubMed], [CAS], [Google Scholar]

10. Liu, J.; de la Garza, L.; Zhang, L.; Dimitrijevic, N. M.; Zuo, X.; Tiede, D. M.; Rajh, T. Photocatalytic Probing of DNA Sequence by Using TiO_2/Dopamine-DNA Triads. *Chem. Phys.* **2007**, *339*, 154– 163, DOI: 10.1016/j.chemphys.2007.07.040 [Crossref], [CAS], [Google Scholar]

11. Chen, W. J.; Tsai, P. J.; Chen, Y. C. Functional Fe_3O_4/TiO_2 Core/Shell Magnetic Nanoparticles as Photokilling Agents for Pathogenic Bacteria. *Small* **2008**, *4*, 485– 491, DOI: 10.1002/smll.200701164 [Crossref], [PubMed], [CAS], [Google Scholar]

12. Vlasova, N. N.; Markitan, O. V. Adsorption of Catecholamines on a Nanocrystalline Titanium Dioxide Surface. *Colloid J.* **2021**, *83*, 203– 210, DOI: 10.1134/S1061933X21020125 [Crossref], [CAS], [Google Scholar]

[PubMed], [CAS], [Google Scholar]

14. Syres, K.; Thomas, A.; Bondino, F.; Malvestuto, M.; Grätzel, M. Dopamine Adsorption on Anatase TiO_2(101): A Photoemission and NEXAFS Spectroscopy Study. *Langmuir* **2010**, *26*, 14548– 14555, DOI: 10.1021/la1016092 [ACS Full Text], [CAS], [Google Scholar]

15. Ronchi, C.; Selli, D.; Pipornpong, W.; Di Valentin, C. Proton Transfers at a Dopamine-Functionalized TiO_2 Interface. *J. Phys. Chem. C* **2019**, *123*, 7682– 7695, DOI: 10.1021/acs.jpcc.8b04921 [ACS Full Text], [CAS], [Google Scholar]

16. Luppi, E.; Urdaneta, I.; Calatayud, M. Photoactivity of Molecule-TiO_2 Clusters with Time-Dependent Density-Functional Theory. *J. Phys. Chem. A* **2016**, *120*, 5115– 5124, DOI: 10.1021/acs.jpca.6b00477 [ACS Full Text], [CAS], [Google Scholar]

17. Jackman, M. J.; Syres, K. L.; Cant, D. J. H.; Hardman, S. J. O.; Thomas, A. G. Adsorption of Dopamine on Rutile TiO_2 (110): A Photoemission and near-Edge x-Ray Absorption Fine Structure Study. *Langmuir* **2014**, *30*, 8761– 8769, DOI: 10.1021/la501357b [ACS Full Text], [CAS], [Google Scholar]

18. Castillo, D.; Ontaneda, J.; Stashans, A. Geometry of Dopamine Adsorption on Rutile (110) Surface. *Int. J. Mod. Phys. B* **2014**, *28*, 1450071, DOI: 10.1142/S0217979214500714 [Crossref], [CAS], [Google Scholar]

19. Cabezas, C.; Peña, I.; López, J. C.; Alonso, J. L. Seven Conformers of Neutral Dopamine Revealed in the Gas Phase. *J. Phys. Chem. Lett.* **2013**, *4*, 486– 490, DOI: 10.1021/jz302135h [ACS Full Text], [CAS], [Google Scholar]

20. López, J. C.; Cortijo, V.; Blanco, S.; Alonso, J. L. Conformational Study of 2-Phenylethylamine by Molecular-Beam Fourier Transform Microwave Spectroscopy. *Phys. Chem. Chem. Phys.* **2007**, *9*, 4521– 4527, DOI: 10.1039/b705614a [Crossref], [PubMed], [CAS], [Google Scholar]

21. Cabezas, C.; Varela, M.; Peña, I.; López, J. C.; Alonso, J. L. The Microwave Spectrum of Neurotransmitter Serotonin. *Phys. Chem. Chem. Phys.* **2012**, *14*, 13618– 13623, DOI: 10.1039/c2cp42654d [Crossref], [PubMed], [CAS], [Google Scholar]

23. Cabailh, G.; Torrelles, X.; Lindsay, R.; Bikondoa, O.; Joumard, I.; Zegenhagen, J.; Thornton, G. Geometric Structure of TiO_2 (110) (1×1): Achieving Experimental Consensus. *Phys. Rev. B* **2007**, *75*, 241403, DOI: 10.1103/PhysRevB.75.241403 [Crossref], [CAS], [Google Scholar]

24. Kröger, E. A.; Sayago, D. I.; Allegretti, F.; Knight, M. J.; Polcik, M.; Unterberger, W.; Lerotholi, T. J.; Hogan, K. A.; Lamont, C. L. A.; Woodruff, D. P. Photoelectron Diffraction Investigation of the Structure of the Clean TiO_2(110) (1×1) Surface. *Phys. Rev. B* **2007**, *75*, 195413, DOI: 10.1103/PhysRevB.75.195413 [Crossref], [CAS], [Google Scholar]

25. Tillotson, M. J.; Brett, P. M.; Bennett, R. A.; Grau-Crespo, R. Adsorption of Organic Molecules at the TiO_2(110) Surface: The Effect of van Der Waals Interactions. *Surf. Sci.* **2015**, *632*, 142– 153, DOI: 10.1016/j.susc.2014.09.017 [Crossref], [CAS], [Google Scholar]

26. Abbaspour Tamijani, A. Weak Binding Mode of CH_4 on Rutile Crystallites from Density Functional Theory Calculations. *Comput. Theor. Chem.* **2017**, *1121*, 11– 28, DOI: 10.1016/j.comptc.2017.09.019 [Crossref], [CAS], [Google Scholar]

27. Calatayud, M.; Markovits, A.; Menetrey, M.; Mguig, B.; Minot, C. Adsorption on Perfect and Reduced Surfaces of Metal Oxides. *Catal. Today* **2003**, *85*, 125– 143, DOI: 10.1016/S0920-5861(03)00381-X [Crossref], [CAS], [Google Scholar]

28. Diebold, U. The Surface Science of Titanium Dioxide. *Surf. Sci. Rep.* **2003**, *48*, 53– 229, DOI: 10.1016/S0167-5729(02)00100-0 [Crossref], [CAS], [Google Scholar]

29. Onishi, H.; Iwasawa, Y. STM-Imaging of Formate Intermediates Adsorbed on a TiO_2(110) Surface. *Chem. Phys. Lett.* **1994**, *226*, 111– 114, DOI: 10.1016/0009-2614(94)00712-8 [Crossref], [CAS], [Google Scholar]

30. Li, S. C.; Wang, J. G.; Jacobson, P.; Gong, X. Q.; Selloni, A.; Diebold, U. Correlation between Bonding Geometry and Band Gap States at Organic-Inorganic Interfaces: Catechol on Rutile TiO_2(110). *J. Am. Chem. Soc.* **2009**, *131*, 980– 984, DOI: 10.1021/ja803595u [ACS Full Text], [CAS], [Google Scholar]

32. Busayaporn, W.; Duncan, D. A.; Allegretti, F.; Wander, A.; Bech, M.; Møller, P. J.; Doyle, B. P.; Harrison, N. M.; Thornton, G.; Lindsay, R. Structure of a Model Dye/Titania Interface: Geometry of Benzoate on Rutile-TiO_2 (110)(1 × 1). *J. Phys. Chem. C* **2016**, *120*, 14690– 14698, DOI: 10.1021/acs.jpcc.6b03991 [ACS Full Text], [CAS], [Google Scholar]

33. Trinh, Q. T.; Bhola, K.; Amaniampong, P. N.; Jérôme, F.; Mushrif, S. H. Synergistic Application of XPS and DFT to Investigate Metal Oxide Surface Catalysis. *J. Phys. Chem. C* **2018**, *122*, 22397– 22406, DOI: 10.1021/acs.jpcc.8b05499 [ACS Full Text], [CAS], [Google Scholar]

34. Ontaneda, J.; Nicklin, R. E. J.; Cornish, A.; Roldan, A.; Grau-Crespo, R.; Held, G. Adsorption of Methyl Acetoacetate at Ni{111}: Experiment and Theory. *J. Phys. Chem. C* **2016**, *120*, 27490– 27499, DOI: 10.1021/acs.jpcc.6b10023 [ACS Full Text], [CAS], [Google Scholar]

35. Tsaousis, P.; Ontaneda, J.; Bignardi, L.; Bennett, R. A.; Grau-Crespo, R.; Held, G. Combined Experimental and Theoretical Study of Methyl Acetoacetate Adsorption on Ni{100}. *J. Phys. Chem. C* **2018**, *122*, 6186– 6194, DOI: 10.1021/acs.jpcc.8b00204 [ACS Full Text], [CAS], [Google Scholar]

36. Quevedo, W.; Ontaneda, J.; Large, A.; Seymour, J. M.; Bennett, R. A.; Grau-Crespo, R.; Held, G. Adsorption of Aspartic Acid on Ni{100}: A Combined Experimental and Theoretical Study. *Langmuir* **2020**, *36*, 9399– 9411, DOI: 10.1021/acs.langmuir.0c01175 [ACS Full Text], [CAS], [Google Scholar]

37. Kresse, G.; Furthmüller, J. Efficiency of Ab-Initio Total Energy Calculations for Metals and Semiconductors Using a Plane-Wave Basis Set. *Comput. Mater. Sci.* **1996**, *6*, 15– 50, DOI: 10.1016/0927-0256(96)00008-0 [Crossref], [CAS], [Google Scholar]

38. Kresse, G.; Furthmüller, J. Efficient Iterative Schemes for Ab Initio Total-Energy Calculations Using a Plane-Wave Basis Set. *Phys. Rev. B* **1996**, *54*, 11169– 11186, DOI: 10.1103/PhysRevB.54.11169 [Crossref], [PubMed], [CAS], [Google Scholar]

39. Blöchl, P. E. Projector Augmented-Wave Method. *Phys. Rev. B* **1994**, *50*, 17953– 17979, DOI: 10.1103/PhysRevB.50.17953 [Crossref], [PubMed], [CAS], [Google Scholar]

41. Monkhorst, H. J.; Pack, J. D. Special Points for Brillouin-Zone Integrations. *Phys. Rev. B* **1976**, *13*, 5188– 5192, DOI: 10.1103/PhysRevB.13.5188 [Crossref], [Google Scholar]

42. Yin, W.-J.; Wen, B.; Bandaru, S.; Krack, M.; Lau, M.; Liu, L.-M. The Effect of Excess Electron and Hole on CO_2 Adsorption and Activation on Rutile (110) Surface. *Sci. Rep.* **2016**, *6*, 23298, DOI: 10.1038/srep23298 [Crossref], [PubMed], [CAS], [Google Scholar]

43. Wei, B.; Calatayud, M. The Subsurface Diffusion of Hydrogen on Rutile TiO_2 Surfaces: A Periodic DFT Study. *Top. Catal.* **2021**, *1*, 1– 11, DOI: 10.1007/s11244-021-01518-w [Crossref], [Google Scholar]

44. O'Rourke, C.; Bowler, D. R. DSSC Anchoring Groups: A Surface Dependent Decision. *J. Phys.: Condens. Matter* **2014**, *26*, 44, DOI: 10.1088/0953-8984/26/19/195302 [Crossref], [Google Scholar]

45. Makov, G.; Payne, M. C. Periodic Boundary Conditions in Ab Initio Calculations. *Phys. Rev. B* **1995**, *51*, 4014– 4022, DOI: 10.1103/PhysRevB.51.4014 [Crossref], [PubMed], [CAS], [Google Scholar]

46. Klimeš, J.; Bowler, D. R.; Michaelides, A. Chemical Accuracy for the van Der Waals Density Functional. *J. Phys.: Condens. Matter* **2010**, *22*, 022201 DOI: 10.1088/0953-8984/22/2/022201 [Crossref], [PubMed], [CAS], [Google Scholar]

47. Klimeš, J.; Bowler, D. R.; Van Der Michaelides, A. Waals Density Functionals Applied to Solids. *Phys. Rev. B* **2011**, *83*, 195131, DOI: 10.1103/PhysRevB.83.195131 [Crossref], [CAS], [Google Scholar]

48. Perdew, J. P.; Burke, K.; Ernzerhof, M. Generalized Gradient Approximation Made Simple. *Phys. Rev. Lett.* **1996**, *77*, 3865– 3868, DOI: 10.1103/PhysRevLett.77.3865 [Crossref], [PubMed], [CAS], [Google Scholar]

49. Anisimov, V. I.; Zaanen, J.; Andersen, O. K. Band Theory and Mott Insulators: Hubbard U Instead of Stoner I. *Phys. Rev. B* **1991**, *44*, 943– 954, DOI: 10.1103/PhysRevB.44.943 [Crossref], [PubMed], [CAS], [Google Scholar]

50. Dudarev, S. L.; Botton, G. A.; Savrasov, S. Y.; Humphreys, C. J.; Sutton, A. P. Electron-Energy-Loss Spectra and the Structural Stability of Nickel Oxide: An LSDA+U Study. *Phys. Rev. B* **1998**, *57*, 1505– 1509, DOI: 10.1103/PhysRevB.57.1505 [Crossref], [CAS], [Google Scholar]

[CAS], [Google Scholar]

52. Grau-Crespo, R.; Schwingenschlögl, U. The Interplay between Dopants and Oxygen Vacancies in the Magnetism of V-Doped TiO_2. *J. Phys.: Condens. Matter* **2011**, *23*, 334216, DOI: 10.1088/0953-8984/23/33/334216 [Crossref], [PubMed], [CAS], [Google Scholar]

53. Chen, H. Y. T.; Tosoni, S.; Pacchioni, G. Adsorption of Ruthenium Atoms and Clusters on Anatase TiO_2 and Tetragonal ZrO_2(101) Surfaces: A Comparative DFT Study. *J. Phys. Chem. C* **2015**, *119*, 10856– 10868, DOI: 10.1021/jp510468f [ACS Full Text], [CAS], [Google Scholar]

54. Thang, H. V.; Pacchioni, G.; DeRita, L.; Christopher, P. Nature of Stable Single Atom Pt Catalysts Dispersed on Anatase TiO_2. *J. Catal.* **2018**, *367*, 104– 114, DOI: 10.1016/j.jcat.2018.08.025 [Crossref], [CAS], [Google Scholar]

55. Birgersson, M.; Almbladh, C.-O.; Borg, M.; Andersen, J. N. Density-Functional Theory Applied to Rh(111) and CO/Rh(111) Systems: Geometries, Energies, and Chemical Shifts. *Phys. Rev. B* **2003**, *67*, 045402 DOI: 10.1103/PhysRevB.67.045402 [Crossref], [CAS], [Google Scholar]

56. Köhler, L.; Kresse, G. Density Functional Study of CO on Rh(111). *Phys. Rev. B* **2004**, *70*, 165405, DOI: 10.1103/PhysRevB.70.165405 [Crossref], [CAS], [Google Scholar]

Cited By

This article has not yet been cited by other publications.